Chapter 11

Fiber Optic–Based Pressure Sensing Surface for Skin Health Management in Prosthetic and Rehabilitation Interventions

Dimitris Tsiokos, George T. Kanellos,
George Papaioannou and Stavros Pissadakis

Additional information is available at the end of the chapter

http://dx.doi.org/10.5772/50574

1. Introduction

1.1. Background and motive

The work presented here responds to the high-prevalence of pressure ulcers and the need for better diagnostic, treatment and prevention practices in the clinic. Factors in pressure ulcer development are classified as intrinsic (e.g. disuse muscle antrophy due to motor paralysis or impaired/absent sensation due to sensory paralysis) or extrinsic (e.g. applied pressure due to external loading to soft tissues, shear due to poor posture and/or poor support materials, or other adverse microenvironment at support interface due to raised temperature, sweating, incontinence, infection). Pressure ulcers are localized areas of tissue breakdown in skin and/or underlying tissues [1], [2]. They can occur in all situations where subjects are subjected to sustained mechanical loads, but are particularly common in those who are bedridden, wheelchair bound or wearing a prosthesis or orthosis. The ulcers are painful, difficult to treat, and represent a burden to the community in terms of healthcare and finances. Consequently, the pressure ulcer problem affects the quality of life of many young and elderly individuals.

It has become apparent that a complete pressure management system integrated with the medical intervention is required in order to measure and redistribute pressure at the human machine interface and prevent the development of pressure ulcer. In this respect, the rapidly evolving field of optical fiber sensing seems to hold a strong potential for providing effective solutions towards accurately measuring and monitoring pressure, strain and shear between the human skin and the support surface [3], [5]. Sensing by means of light offers a number of advantages when utilizing the appropriate fiber sensor configuration, since light

propagation is highly sensitive to external forces and perturbations yielding real-time measurements with almost negligible hysteresis [6]-[8]. In addition, optical fibre sensors provide immunity to electromagnetic interference, high sensitivity, small size and low weight, passiveness, resistance to harsh environments, multiplexing capabilities and possibility to parallelize the readout. Equally important is that optical fiber based pressure sensors can in principle confront with true medical requirements as real time data acquisition, high sensing resolution and increased dynamic range. These fiber sensing properties have turned photonic sensing technology into more versatile and often more reliable than its electronic counterparts and have been already identified and utilized in a number of applications in diverse fields. Structural health monitoring, automotive industry, oil and gas extraction, aeronautics and aerospace, robotics, healthcare, etc. have already adopted fiber sensor configurations in several crucial sensing functionalities, but unfortunately only minor attempts have been pursued towards synergizing the field of photonic sensing with biomechanics, orthopaedics and rehabilitation [9]-[11].

Being fully aware of this new technological sensor toolkit, our work is born out of the need for readdressing a number of traditional challenges in support surfaces and prosthetics by taking advantage of, and effectively integrating recently available technological advances that offer the opportunity to tackle previously unresolved problems. That is, integrate knowledge in photonic sensing with rehabilitation engineering and biomechanics in order to address the unanswered question of pressure ulcer development in the human-machine interfaces of biomedical interventions.

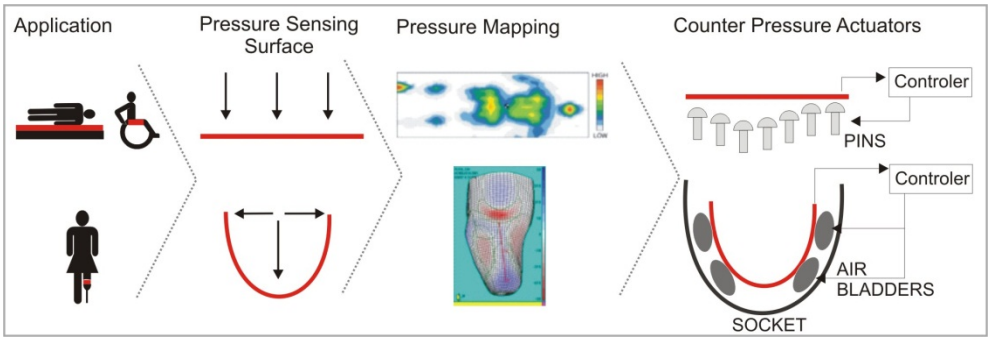

Figure 1. Schematic of the pressure management system proposed for both cases of bed/seating system sensing surface (top row) and lower extremity prosthetic socket sensing surface (bottom row). The first step involves the measurement of the pressure loads across the sensing surface, then generate pressure maps that define pressure distribution and finally drive counter pressure actuators to redistribute pressure across the surface for pressure relief.

The pressure sensing system that we are describing in this chapter aims to be embedded in a pressure management expert system that is presented in fig. 1. Specifically, in order to maintain skin health at areas of the skin that prolonged pressure loads are applied, a pressure tension relief is introduced in order to redistribute pressure and relief any excessive pressure or tension applied on the skin by means of a sensor matrix and counter

pressure controllers and actuators. The pressure management system can be customized to be applied in medical beds or seating systems (wheelchair) and prosthetic sockets in lower extremity prosthetic interventions as depicted in fig. 1. A dynamic control system of supporting pins for the bed and seating system or air bladders for the prosthetic socket will anticipate with the help of feedback of fiber optic pressure sensors, points of high pressure at the human-machine interface (HMI) and will locally decrease pressure in the material at those locations before those pressure thresholds are reached in real time. Pressure redistribution protects tissues against prolonged and excessive epidermal pressure developed in the HMI. This will in turn prevent the onset or deterioration of pressure ulcers.

To this end, we are reporting on the development of a flexible 2D optical fiber-based pressure sensing surface suitable for human machine interfaces in biomedical and rehabilitation applications. The sensor comprises of highly-sensitive Fiber Bragg Grating elements embedded in a thin polymer sheet to form a 2x2 cm^2 sensing pad with a minimal thickness of 2.5mm, while it is easily expandable in order to be used as a building block for larger surface sensors. The fabricated pad sensor was combined with a low physical dimension commercially available interrogation unit to enhance the portability features of the complete sensing system. Sensor mechanical properties allow for matching human skin behavior, while its operational performance exhibited a maximum fractional pressure sensitivity of 12 MPa^{-1} with a spatial resolution of 1x1cm^2 and demonstrates no hysteresis and real time operation. In parallel, in order to maximize sensing surface durability while maintaining functional properties we conducted mechanical tests in three different case studies through which we identified the optimized fabrication properties (thickness, fiber positioning depth, fiber type) of the sensing surface.

More specifically, the chapter is organized in five different sections. The rest of the first section describes the state-of-the-art in pressure sensing technologies while the FBG sensor presented in this chapter will be briefly benchmarked against currently available technologies. Section 2 presents the principle of operation of the proposed pressure sensing scheme. The development of the optical fiber 2-D pressure sensing pad takes advantage of the highly sensitive 1-D Fiber Bragg Grating (FBG)-based array structures, which are arranged in a 2-dimensional sensing surface. Section 3 will describe the experimental proof of concept of the concept presented in Section 2 and the results obtained in the experiment. Section 4 presents a sensor optimization study that was performed in order to optimize the sensor operational features versus its mechanical and structural properties. We have identified the basic fabrication parameters that will enhance sensor pads rigidity and durability to guarantee the sensor pads reliability. These parameters are: optical fiber grating optimum inscription characteristics, optical fiber type (hydrogenated/non-hydrogenated fiber), depth of fiber embodiment in the polymer (hosting) material and thickness of the polymer sheet. We have performed a thorough analysis of these parameters and the results will be presented and discussed in this section. Section 5 will describe in more detail the application perspective of the developed sensor. The targeted technological applications will be discussed including medical beds, wheelchairs and lower extremity below-the-knee prosthetic sockets while the required characteristics and specifications of the

sensing surface per application will be highlighted. Finally Section 6 will describe the summary of the chapter and the conclusions obtained.

1.2. State-of-the-art in pressure sensing technology

Efforts to prevent pressure ulcer development are plagued with inconsistencies and a general lack of best practice guidelines. For instance, repositioning patients in medical beds is still the most common approach used in an attempt to prevent the development of pressure ulcers, but additional measures are diverse. The monitoring of magnitude and timing of all the extrinsic parameters requires a mere quantitative assessment of the pressure profile at a given time. Information of the potentially ever-changing multidirectional loading patterns in real time is still an unresolved HMI sensing issue.

The variety of research transducers for pressure measurements are classified based on their operation principle [12]-[15], [16], [17] as fluid-filled sensors [18], pneumatic sensors, diaphragm deflection strain gauge [19], cantilever/beam strain gauge, MEMS and printed circuit sheet sensors [18]-[25]. The most commonly used, in- vivo clinical pressure sensors (capacitive, piezoelectric, ink-film based) are the Tekscan (Boston, MA), the Xsensor (Calgary, Canada), Schönefeld, (Germany), the Vista medical (Winnipeg, Canada), the Rincoe Socket Fitting System and the Novel (Munich, Germany) [20]-[32] (see table 1). Industrial equivalents include "Bodyfitter" by Sensor Products (Madison, NJ), ElekSen (Iver Heath Bucks, UK), Pressure Profile Systems Inc. (Los Angeles, CA). The underlying technology of these products is basically the measurement of a certain material's conductivity as it changes with pressure [33]. However, these sensors possess many disadvantages such as accuracy, hysteresis, signal drift, the response to curvature, spatial resolution and temperature sensitivity [20]-[32]. An ideal system should be able to monitor real interfacial stresses continuously, solve the associated data acquisition and conditioning issues, and allow placement at the assistive device interface without significant obstruction to the original boundary conditions. These sensors are conditioned for low pressure and short-term applications, and are therefore not addressing sensor creep. So for the consistency of results (i.e. drift compensation) a post processing of the raw data is always recommended but not available in current products. This rather laborious process is associated with the known variances of particular sensing elements and must be simplified if these instruments reach the clinical field. In addition to that, it seems almost impossible to calibrate and monitor in real time electrical, piezoresistive and capacitive systems for conditions where the sensor carrier is bended, stretched or bulged [13], [15]. A study [34] found that the Tekscan system overshoot readings that were applied in areas smaller than 4 cm^2, showed substantial hysteresis (+20%), drift and creep (19), but still is preferred by clinicians for its real time display capabilities and resolution. Other studies compared commercial systems for accuracy and repeatability (Talley pressure electropneumatic Evaluator-Talley Medical, UK, DIPE-Next Generation CA, US [13]-[15], [33], Force Sensing Array, FSA-Vista Medical, Canada) and reported problems with accuracy, repeatability, speed, data presentation, pronounced hysteresis (+14-25%) and significant creep (12%) [33]. They were also shown to underestimate the force applied on a small contact area (less than 4

cm^2). In all of these evaluations one common observation was the inability of the sensors to comply with large radii of curvature and surfaces with very complicated geometry. Sensor protrusion into the skin was another notable limitation since it caused erroneously high measurements in these latter studies.

To summarize the above analysis, it becomes obvious that there is currently no system that manages simultaneously micro-controlling of pressure management and higher-level ergonomic adaptations in a real time dynamic environment in the arena of pressure management devices. With respect to the sensing elements adopted so far, severe limitations in pressure ulcer diagnosis can be attributed to poor sensor accuracy, consistency (sensor drift and hysteresis) and calibration reliability. These factors are also mainly responsible for the absence of a reliable sensing system that will be able to report real time measurements of the potentially ever-changing multidirectional loading patterns in human/machine interface issues.

1.2.1. Optical fiber pressure sensors

Limited work has been done in the field of healthcare towards synergizing photonic sensing with biomechanics, orthopaedics and rehabilitation applications. Within these attempts, a FBG-based pressure sensor has been demonstrated in the design of a high-resolution optical fiber manometry catheter [35]. On the other hand, fiber optic surface sensing structures for health-care pressure measurements have not yet been adequately addressed. To this end, a 2D fiber-sensing configuration was presented by Chu-Yu Huang et al. [36], where a 2D mesh of simple optical fibers embedded in a silicon-polymer material was used to assess shoe insole pressure, exhibiting however low sensitivity.

Efforts in fabricating a 2D fiber sensing configuration with increased sensitivity are also currently being deployed in [37]. The measurement of mechanical quantities using optical fibers and Bragg grating (FBG) sensors as considered here relates to forces that act transversely upon the optical fiber cladding. A variety of sensing mechanisms that convert either a transverse line load, a hydrostatic pressure (in case of a bare optical fiber) or a transverse load (on an embedded optical fiber) into an optical quantity that can be encoded in the Bragg peak wavelength of a FBG reflection signal have been proposed.

A first method hosts the FBG in a mechanically asymmetric birefringent optical fiber. The mechanical load is then directly encoded in the spectral separation of the two Bragg reflection wavelengths returned by the FBG. The most straightforward implementation of a mechanically asymmetric birefringent optical fiber is the side-hole fiber (with elliptical core) first demonstrated by Xie et al. in 1986 [38]. In 2007, Jewart et al. demonstrated the Bragg grating sensing characteristics of a side-hole fiber with large airholes [39]. The high transverse line load sensitivity of 176 pm/(N/mm) that was reported for the peak separation shows that optimizing the transverse sensitivity of optical fibers is possible with an adapted cross-section. Despite its high sensitivity to transverse loading, this sensor starts to work after a certain non-zero transverse line load while it does not allow achieving a high birefringence without significantly increasing their temperature sensitivity. Dedicated

microstructured optical fibers (MOF) provide a solution to those difficulties. The experimental results published so far indicate that the sensitivity to temperature in highly birefringent MOFs strongly depends on the fiber geometry and can be up to 3 orders of magnitudes lower than in standard elliptical core fibers [40]-[44]. However, the sensitivities obtained with these MOF are still not sufficient in view of the required pressure measurement resolutions imposed by HMI demanding applications in medical mattresses and prosthetic sockets.

	X Sensor	FSA	Tekscan	Talley	Pressure	Novel	FBG-based
Principle of operation	Capacitive	Piezo-resistive	Resistive	Electro-pneumatic	Pneumatic	Capacitive	OPTICAL
System	Seat Mattress	Seat, Back, Bed, In shoe, Orthotists	Seat, In shoe, Dental	Individual sensor	Individual sensor	Seat, Foot, Specialst e.g. bike seat hand	Matress, whellchair, seat, socket
Sensor size (mm)	Seat 12.5x12.5 Hi-res 2.7x2.7	Bed 19x50 Foot 9x16	Foot 5x5	100 mm round 28 mm round	25 or 62.5	2.7x2.7 min 31x47 max	1000x1000
Sample rate	Up to 70,000 Sensors s-1	3,072 sensors s-1	316,800 sensors s-1	N/A	N/A	Up to 20000 sensors s-1	Real-time
Range (mmHg)	0-220	Bed 0-200 Foot 0-1500	Seat 0-200/1,000 Foot 0-7500	20-300	0-125	Bed 0-200 Foot 0-1,800	At least 3000
No of sensors	Seat 2304 Bed 10,240 Hi-res 65K	Up to 32x32	Over 2,000	1	1	Up to 2,304	4 or 8
Quoted Accuracy	10% or 10 mmHg	10%	Clin. ± 3% Lab. ± 1%	± 2%	±3 mmHg	Typically ±5%	Unknown
Output device	Computer	Computer	Computer	Handheld digital gauge	Handheld digital gauge	Computer	Interrogator

Table 1. Comparison of commercially available interface pressure measuring systems vs the targeted proposed sensing scheme

2. Proposed pressure sensing concept

In this section, we describe the development of a 2D optical FBG-based pressure sensing surface that combines the advantages of the FBG-array sensors with novel, elastic and flexible Polydimethyl-siloxane (PDMS) polymer material to provide a light-weight, compliant and flexible 2D pressure sensing surface. The sensor comprises of highly-sensitive Fiber Bragg Grating elements embedded in a thin polymer sheet to form a 2x2 cm^2 sensing pad with a minimal thickness of 2.5mm, while it is easily expandable in order to be used as a building block for larger scale sensors. The sensor's enhanced performance exhibited a maximum fractional pressure sensitivity of 12 MPa^{-1} with a spatial resolution of 1x1cm^2 while it demonstrated no hysteresis and real time operation. The mechanical properties of this pad sensor makes it very unobtrusive while they allow for wrapping, embedding or attaching the sensor to irregular shapes and geometries, offering enhanced response to curvature. The fabricated pad sensor was combined with a low physical dimension

commercially available interrogation unit interrogation unit [47] to enhance the portability features of the complete sensing system. The physical and operational characteristics of the presented pad sensor and particularly its high sensitivity in low absolute pressure values, its high spatial resolution and unobtrusive characteristics combined with potential portability are ideally suited for biomedical applications including amputee sockets, shoe sensors, wearable sensors, wheelchair seating-system sensors, hospital-bed monitoring sensors and other ergonomics sensors.

The development of the optical fiber 2-D pressure sensing pad takes advantage of the highly sensitive 1-D FBG-based array structures, which are arranged in foils as shown in Fig. 2(a) to form a 2-dimensional sensing surface. The foiled optical fiber sensor elements are embedded in a thin silicon polymer material to form an elastic sensing sheet. Based on the intensity modulation caused Bragg wavelength shifting, induced by the bending of the embedded fibers, a map of displacement or force over an area is generated. The pressure is obtained from the force applied on each sensing point divided by its effective area. Multiplexed FBG array configurations are used to address applications that require multipoint monitoring of the applied external forces, where every respective FBG element comprises a single point of measurement. As shown in Fig. 2(a), longitudinal spacing d of the FBGs defines the axial spatial resolution of the linear sensor.

The 2D surface sensing is obtained by proper arrangement of FBG arrays in 2D structures, as shown in Fig. 2(a), built on a flexible and stretchable silicon-polymer Polydimethyl-siloxane (PDMS) sheet. PDMS is suitable for sensing applications to match ideal skin behavior, since it is flexible, stretchable/elastic and with controllable viscosity and hardness. This pad can be wrapped around, embedded in, attached and anchored to irregularly shaped and/or moving objects or bodies and allows quasi-distributed sensing of mechanical quantities such as deformation, pressure, stress or strain along the entire surface. 2D spatial resolution is now defined by the fiber axial sensor distribution d and the spacing of optical fibers D. The presented 2D pressure sensor concept may be arranged as a uniform large scale surface (Fig. 2(a)), or may be implemented as an assembly of small scale building blocks that are properly interconnected, as shown Fig.2(b). The second approach gives the advantage of increased sensor shape flexibility while decreasing manufacturing complexity, that comes however at the expense of increased connectorisation and surface sensing discontinuities. In the present communication, we report on the implementation and evaluation of a 2x2 cm^2 sensing surface serving as a building block for larger scale sensors [48].

WDM interrogation method allows for multiplexed sensor networks as each is assigned a given “slice” of the input broad-band light spectrum. We make use of a novel interrogation unit [47] that features miniaturized properties, such as a weight of 150g , power consumption of <0.25 W and physical dimensions in the order of cm (LxWxD; 7x4.6x1.8 cm) while exhibiting a maximum operational frequency of 2.5 kHz for both wavelength shift and FBG central wavelength power loss measurements, an operational dynamic range of 32nm with 5pm resolution, to highlight the potential of implementing a fully portable highly sensitive sensing system.

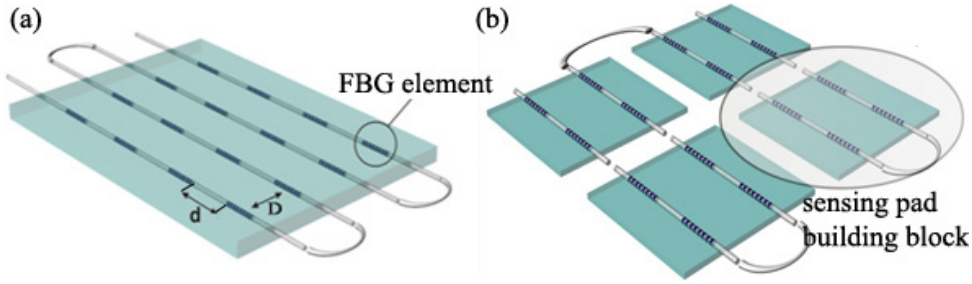

Figure 2. a) PDMS 2D sensing surface with FBG-array optical sensing elements b) elementary 2D sensors used as building blocks for large scale surface sensors

3. Experimental demonstration

3.1. Experimental setup

A fundamental four element (2x2) FBG-based sensing surface of Fig. 2(b) is implemented by intersecting 2 rows of optical fiber patchcords, each bearing an array of 2 FBG acrylate coated sensors. The length of each FBG sensing element is 5mm and their longitudinal spacing d is fixed to 5mm, while optical fibers are spaced D=1cm, leading to a total sensing area of 2x2 cm^2. The optical fiber sensors are embedded in the PDMS material with a nominal elasticity of E=650 kPa (Young's Modulus) so as to produce an elastic sheet of 2.5 mm thickness exhibiting a maximum allowable bend radius of 20 mm. When optical fibers are embedded into the elastic PDMS material, the effective material properties of the fiber reinforced composite (i.e. homogenized average properties which can be measured experimentally) can be assumed to be linear anisotropic if deformation is small and both materials are within the linear region. Full characterization of the effective material properties of the heterogeneous composite structure can be addressed using a series of static FEA solutions [49].

For the fabrication of the sensing pad we used acrylic sheets with etched molds and holders for the optical fibers, as shown in Fig. 3a. A CO laser system (laser beam μm) was used to etch 250 μm depth fiber trenches on 2.5-mm-thick acrylic boards. The optical fibers were assembled on the acrylic top board to create the composite optical FBG sensor. Then a PDMS elastomer (RTV 615 silicone elastomer made by Momentive) mixture was prepared by mixing the copolymer with a curing agent (10:1 ratio). The produced PDMS was poured into the mold, and the composite was placed in vacuum for 24 h to remove any air sensors was completely cured. The PDMS-based sensing pad was finally lifted away from the acrylate board after it was cured. The optical part of the experimental setup is depicted in Fig. 3(b). A Superluminescent-LED source was used to power the FBG elements of the sensing pad, while an optical coupler fed the back-reflected light to the Ibsen I-MON 80 D interrogation unit. A NI DAC card installed in a PC was used to read the extracted data.

In order to evaluate the sensor performance, a series of vertical load tests were conducted throughout the total surface of the pad sensor using a gauge test stage. A Material Tester

system, the MTS 858 Mini Bionix II, was used to apply vertical force and displacement to the prototype sensor through a force gauge with a pin-head of 1cm² (fig.5a) and a universal motion controller. The resolution of the applied displacement stage was 1μm with a force gauge resolution of 10 mN.

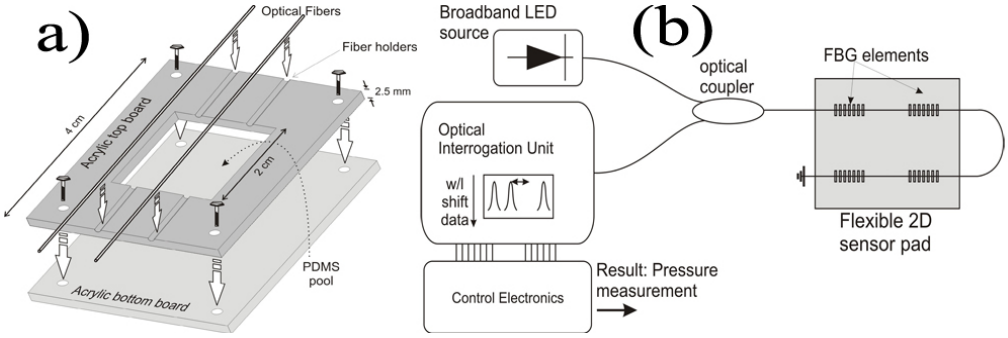

Figure 3. a) Schematic description of the fabrication procedure for the 2x2 FBG element sensor b) experimental setup of the optical circuitry

3.2. Results

Figure 4(a) shows the power spectrum for all four FBGs before (blue line) and after (red line) a load was applied to FBG 3. In the blue spectrum, each peak represents the corresponding centre (Bragg) wavelength of each FBG element (4 in total) when no forces are applied. The FBG wavelengths are spaced 2nm apart, while the total wavelength range of the 2x2 sensing pad is 8nm as shown in Fig. 4(a). Each Bragg wavelength peak represents a single pressure monitoring point exhibiting a FWHM bandwidth of 0.5 nm with sidelobe suppression greater than 17dB. When vertical force or displacement is applied to a FBG element, its Bragg wavelength is shifted. In our experiment the sensor was placed on a metal table with stable temperature, to isolate the sensor from temperature variations. Temperature independent operation can be also obtained by employing an additional FBG sensor that will be responsible solely for temperature sensing without being affected by pressure. More specifically, as the proposed 2x2 pressure sensor is intended for Human-Machine interface systems in biomedical applications, sensor temperature variations will result to roughly the same wavelength shift to all FBGs. This common wavelength shift can be perceived as an offset to the pressure induced resonance shifting, which in turn can be quantified by means of the additional FBG sensor that should be located outside the pressing area acting as the temperature reference sensor. Once this offset has been quantified, sensing pad temperature calibration can then be obtained by removing this offset from the pressure-induced wavelength shift measurements.

The red spectrum of Fig 4(a) depicts the power spectrum of the four FBG sensor elements when 400μm of vertical displacement corresponding to 5N force was applied to FBG3. As

shown, the force applied to FBG3 produced a shift of 0.4 nm to the central wavelength of FBG3 while small variations in the FBG 2 and 4 spectrums are due to the crosstalk between the 2nm spaced FBG channels and their sidelobes overlapping.

The wavelength shift of FBG3 corresponds to 5.188x10-3 MPa^{-1} fractional pressure sensitivity. From the same graph, a power-loss of more than 60% was measured for the central wavelength of FBG3 corresponding to a power loss fractional pressure sensitivity of 12 MPa^{-1}. The power-loss method significantly increases the sensor sensitivity due to the autocorrelation function between the FBG filter envelope and the detection filter of the interrogator CCD pixel. However, increased sensitivity comes at the cost of restricted dynamic range, limiting the wavelength shifting tolerance of our method to the FWHM of the FBG power spectrum. A conventional wavelength shift measurement method may be applied for larger pressure values that correspond to increased wavelength shifts.

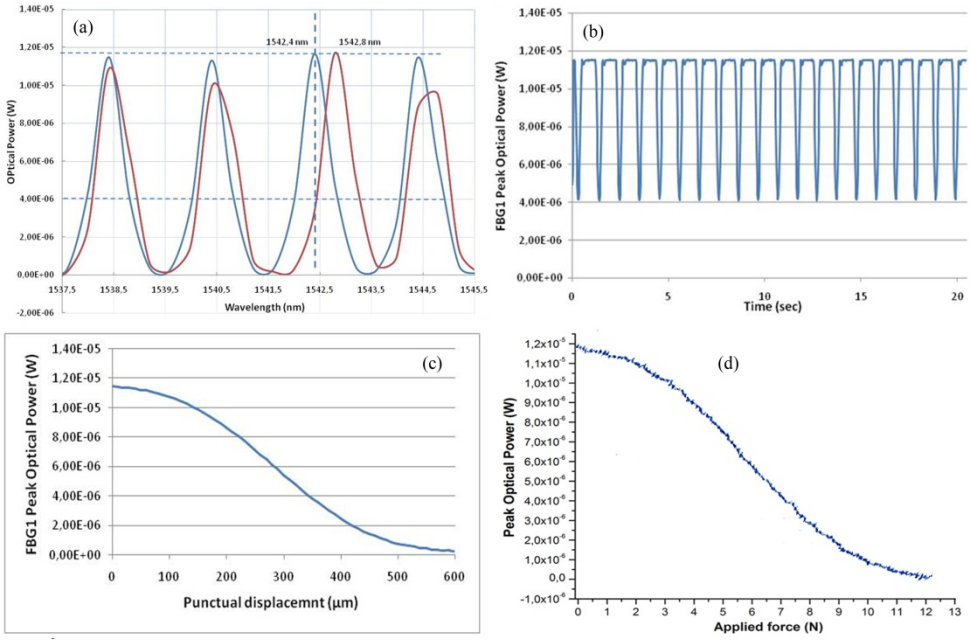

Figure 4. (a) Power spectrum for the 4-FBG sensor: blue line: without any axial load, red line: vertical displacement applied to FBG3. A wavelength shift occurs b) Cyclic loading test: Power loss trace for FBG1 for 400μm vibrating displacement applied c) Power loss vs vertical displacement for FBG1 (Ramp measurement) d) Power loss vs force for FBG1

In order to evaluate the measurement repeatability capability of the sensing pad, we conducted vertical load tests for each FBG element using a 1 cm^2 –head pin in a cyclic pattern. Specifically, we repeatedly tested the sensor by using a vibrating pin to apply a vertical maximum displacement of 400μm to FBG1 at 10Hz, corresponding to 5N force or 50 KPa of pressure.

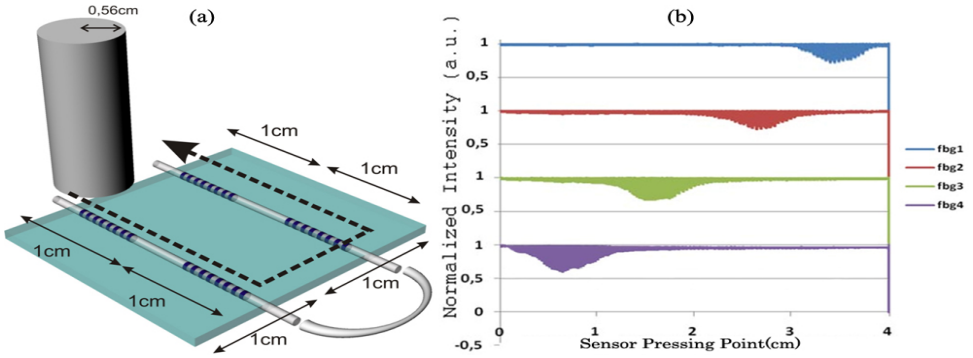

Figure 5. a) Schematic of 2x2 sensor and sliding under the pin b) Simultaneous measurement of 4 FBG normalized intensities vs the position of the pin.

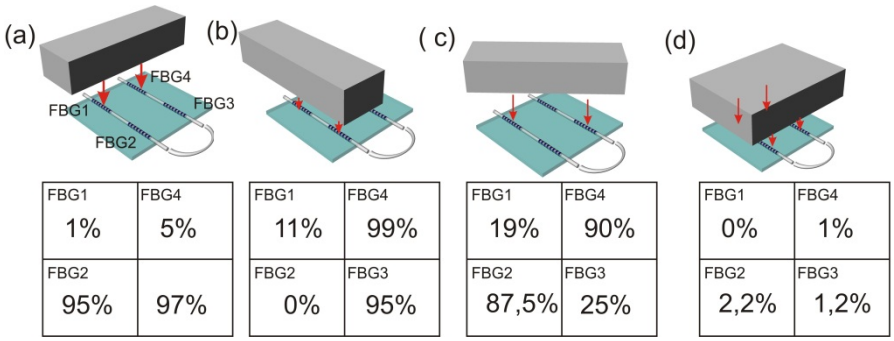

Figure 6. a) Schematic of 2x2 sensor and sliding under the pin b) Simultaneous measurement of 4 FBG normalized intensities vs the position of the pin.

Figure 4(b) shows the optical power measurements versus time for FBG1 Bragg wavelength obtained by means of an optical photodiode. Power loss sensitivity of 60% is confirmed for every duty cycle of the vibrating pin. The graph demonstrates the fast response of the sensing system to the cyclic force pattern applied with negligible hysteresis. A short dumped oscillation of the optical power appears at the end of every wave cycle on the graph. Due to its adhesive and visco-elastic characteristics, the PDMS is locally pulled upwards by the pin beyond the PDMS surface level whenever (i.e. every 1 sec) the pin returns to its starting position. When the PDMS detaches from the pin, it returns to its resting position through a damped oscillation. The oscillation translates into stress oscillation of the corresponding FBG and eventually appears as an optical power oscillation at the end of every cycle of the graph shown in Figure 4(b). Ramp measurements with step increment of vertical displacement were also performed to identify the FBG sensors' dynamic range using the power loss method. Figure 4(c) depicts the Bragg wavelength peak power of FBG1 versus displacement and the corresponding force (Fig. 4(d)). Step increment of displacement was set to 10 μm with overall ramp duration of 1sec. Figures 4(c,d) reveal a dynamic range of 600μm displacement, 10 N of force or 100kPa of pressure and a near-linear

sensitivity of 10% power loss per 1N (10 kPa). Similar results were obtained for each of the four FBG elements.

Sensing elements for distributed pressure sensing systems have to operate independently. In particular, 1:1 mapping of each pressure reading to the corresponding point under pressure, will avoid complex mathematical post-processing of the results. To verify the independent operation of each FBG sensing element in our configuration, we slid the 2x2 fiber optic sensing pad in a circular manner under a vibrating pin with 1 cm2-rounded head, as shown in Fig. 5(a). The pin vibrated at a frequency of 10 Hz and a peak-to-peak vertical displacement of 250 μm. We simultaneously measured the peak power of each FBG Bragg wavelength and the result is depicted in Fig. 5(b). The horizontal axis of Fig. 5(b) refers to the relative pressing point in cm as the pin moves over the FBGs, while normalized intensity values are used for the FBG Bragg wavelengths to compensate for the different mean optical powers between the two fiber optic patch-cords. The result clearly shows independent operation of each FBG sensor within the 1cm fiber axial length, while the spatial resolution of the FBG sensing elements is calculated to as low as 1 cm^2.

In order to study the fiber-based sensor operation under more realistic conditions, we tested the sensor in multipoint operation using a rectangular metal bar with 1cm edge to press all possible 2-point combinations and a metal plate with a surface larger than the total sensor to press all four sensing points. The metal patterns were set to vibrate at a frequency of 10 Hz and for a peak-to-peak displacement of 600μm, driving the sensing elements to their operational limits. Figure 6 (a),(b),(c),(d) depict some of these cases along with the tables indicating the percentage of optical power received for each FBG wavelength at the moment of maximum displacement. In Fig. 6 (a),(b),(d), small variations in the indicated FBG power losses are due to the slightly different response of each FBG. Fig. 6(c) shows that aside from FBGs 1 and 3, small power losses occur in FBGs 2 and 4 due to unwanted partial overlapping between the 1cm metal bar and the latter FBGs. However, clear identification of the multipoint pattern is still allowed. Finally, it should be noted that while the fiber deformation mechanism for the pin-based experiments relies on fiber bending, in Fig. 6(d) the axial extension of the FBGs is due to the Poisson effect material expansion of the PDMS that exhibits a Poisson ratio nominal value of 0.5.

4. Sensor optimization - Comparative studies

4.1. Purpose of the case study

With this work we aim to bring optical fiber sensing closer to their deployment in rehabilitation applications, such as medical beds, wheelchairs and amputee sockets. The developed polymer material pressure sensor pads with embedded FBG elements have to confront with true medical requirements as real time data acquisition, high sensing resolution and increased dynamic range but also requiring a number of fabrication, packaging, manufacturing and operational challenges underlined by the large diversity of the patients to be treated (human factor) and the increased variability of patients' real life

conditions. Specifically for the medical mattress bed and wheelchair application, sensor pads applied on the human–machine interface surface must withstand excessive instant stresses that occur by the patients spontaneous movements. As such, the rigidity of the sensors employed and their permanent damage threshold should far exceed their operational limits, in order to guarantee their sustainability. In this paper, we identify the basic manufacturing parameters that will enhance sensor pads rigidity and durability to guarantee the sensor pads reliability. These parameters are: optical fiber grating optimum inscription characteristics [50], optical fiber type, depth of fiber embodiment in the polymer material and thickness of the polymer sheet [45]. We have also performed a thorough analysis of these parameters and the results are presented and discussed here. We concluded that optimum sensor pad layout that enhances durability and preserves required sensitivity is fiber embodiment at the polymer center with thickness 3mm [51].

4.2. The specimens

The main fabrication parameters that affect the FBG rigidity and durability are the depth of fiber embodiment in the polymer material, the thickness of the polymer sheet and fiber type and grating inscription method.

Hydrogenation of the optical fibre minimizes the inscription time, but also severely limits the strength of the fibre. In this article we perform comparative tests between hydrogenated and non hydrogenated fibers to study their durability behavior. Commercial, standard-NA, Ge-doped enhanced photosensitivity –non-hydrogenated fibres were used. This choice was carried out with respect to the laser sources available and the photosensitivity they induce. Furthermore, suitable choice of the laser wavelength defines the grating inscription time and energy accumulation in the optical fibre body. Between the 248 and 193 nm nanosecond excimer laser ultraviolet sources, it was proved that by using 193 nm laser radiation, strong Bragg reflectors can be straightforwardly inscribed in commercially available standard NA germanosilicate fibres. 193nm excimer laser radiation excites structural and electronic defects lying near the band-gap of the germanosilicate core, rendering the inscription process dependent upon several types of pre-existing defects, while allowing high inscription yield [52][53].

Specifications	**SMF 28e**	**GF1B**
Second Mode Cut-off	≤1260 nm	1260 ± 100 nm
Bend loss @ 1550 (100 turns)	0.03 dB (50 mm mandrel radius)	0.09 dB (25 mm mandrel radius)
NA	0.14	0.13
Proof Test Level	≥ 100 kpsi (0.7 GPa)	≥ 100 kpsi (0.7 GPa)
Operating Temperature	- 60 ^{o}C to +85^{o}C	- 55 ^{o}C to +85^{o}C
Coating Material	UV Cured, Dual Acrylate	UV Cured, Dual Acrylate
Price	0.2 € per metre	4 € per metre

Table 2. Specification and cost data for the smf 28e and gf1b fibres considered

Commercially available photosensitive optical fibres were reviewed, while considering cost parameters, photosensitivity behaviour, splicing losses, mechanical properties and laboratory handling. In such an investigation these fibres were exposed using a variety of laser wavelengths and exposure conditions for illustrating the optimum Bragg grating recording envelope with respect to mechanical strength and grating spectral characteristics.

After considering the data of Table 2, we concluded that two fibres should be further investigated: SMF-28e (drawn by Corning Inc.) and GF1B (drawn by Nufern) [50]. Specification and cost data for those two fibres appear in Table 2.

For the inscription of the FBGs the phase mask technique was used employing an ArF excimer laser emitting at 193nm. A versatile experimental set up was developed for maintaining high robustness and stability over long exposure periods. A custom made phase mask holder and a tension gauge system allow the straightforward recording of concatenated Bragg gratings of different periods and strengths, over different spatial positions in a single optical fibre. Further equipment is currently embedded into the setup for gaining the capability to perform grating apodization. Table 3 summarizes the specifications of the developed FBG. Both fiber type FBG sensors have been embedded in a series of polymer sheet specimens in order to allow the mechanical behavior studies versus two key manufacturing parameters: thickness of the polymer sheet and fiber embodiment depth.

Specifically, specimens employing polydimethyl-siloxane (PDMS) RTV-615 polymer material were fabricated with their thickness ranging from 2mm to 3mm. The two fiber types FBG sensors are embedded in the middle of the PDMS sheet for each specimen (Fig. 7.b). Measurements of the two fiber types on the same sensor pad configuration will provide a first comparison study for the two types of fabricated FBG. Measurements will be taken using the wavelength shift method around the FBG sensor at positions 1cm away from the sensor and the sensors will be driven to their permanent damage limits.

Characteristics	**SMF28e**	**GF1B**
FBG Length	2 mm	2mm
Energy density	166 mJ/cm^2	166 mJ/cm^2
Laser frequency	40 Hz	40 Hz
Inscription time	25 min	2min 40 sec
Accumulated fluence	597.6 K J/cm ^{2}	63.7 K J/cm ^{2}
FBG strength	10.23 dB	10.45
Side lobe suppression (non optimized set-up)	5 dB	5 dB

Table 3. FBG specifications for both fiber types

The effect of fiber embodiment depth in the PDMS towards the mechanical and operational characteristics of the sensor pads is studied using specimens of Fig. 7.a. The specimens exhibit thickness of 2mm and 3mm while the two fiber sensors where of the same type. The fibers are embedded one in the mid-depth of the PDMS and the second is positioned close to the PDMS surface (400μm). This configuration will allow for characterizing the sensors behavior when sensors are embedded in the top/bottom surface of PDMS.

The sensor pads fabrication procedure employs specially designed metal plates or acrylic boards where the optical fibers are positioned to create the composite optical FBG sensor. PDMS elastomer (RTV 615 silicone elastomer made by Momentive) mixture is prepared by mixing the copolymer with a curing agent (10:1 ratio). The mixture is placed in a vacuum system to remove any air bubbles that have been formed during mixing. The produced PDMS is poured into the mold, and the composite is placed in vacuum for 24 h until the PDMS sheet with the embedded FBG sensors was completely cured. Fig. 7(d) depicts a photograph of the sensor.

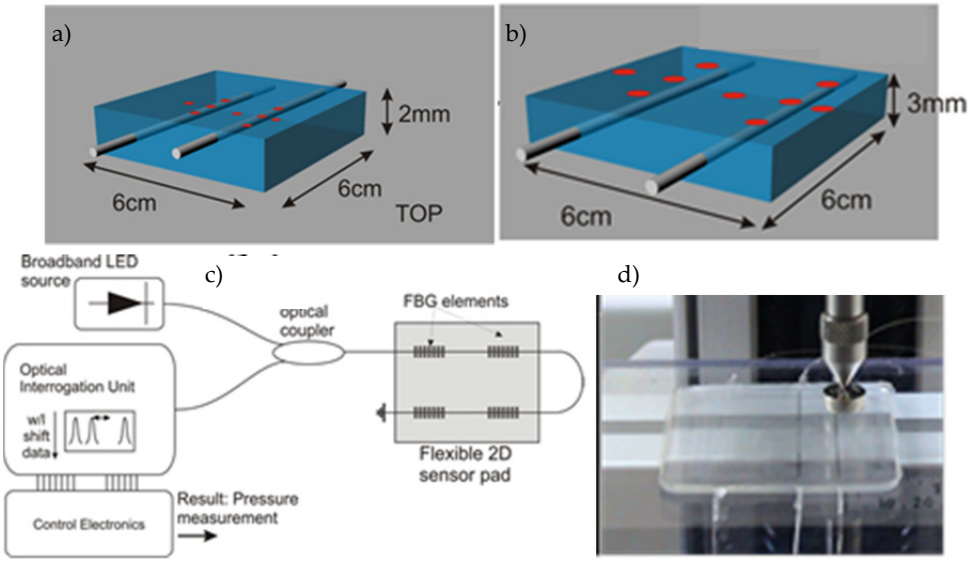

Figure 7. a) Fiber embodiment depth study specimens b) thickness study specimens c) optical part of experimental setup d) photo of specimen under test

4.3. Experimental setup

The optical part of the experimental setup is similar to the one used in the first experiment in Section 2 as depicted in Fig. 7(c). A Superluminescent-LED source is used to power the FBG elements of the sensing pad, while an optical coupler fed the back-reflected light to the AOS interrogation unit. In order to evaluate the sensor performance, a series of vertical load tests were conducted using a gauge test stage. A Material Tester system, the Mcmesin i5, was used to apply vertical force and displacement to the prototype sensor through a force gauge with a pin-head of $1cm^2$ (Fig. 7(d)). A conical pin is pressing a $1cm^2$ round metal plate with rounded edges to guarantee homogeneous pressure distribution.

4.4. Comparative studies' results

In this section we present the results for the three different case studies (embodiment depth, thickness and fiber type) with respect to FBG sensors sensitivity and their dynamic range of ultimate damage point.

4.4.1. Fiber embodiment depth study

Figure 8 presents the results obtained for hydrogenated SMF-28 fiber FBG sensors when embedded in a 2mm thick PDMS sheet in the center and top position of the cross-section. The results reveal a 50% increased sensitivity and a 40% increased durability for the FBG positioned in the center of the PDMS layer.

4.4.2. Thickness study

Figure 9 presents the results obtained for hydrogenated SMF-28 fiber FBG sensors when embedded in 2mm and 3mm thick PDMS sheets respectively. Again an increased sensitivity of 50% and a marginal increase of durability are evident for the thicker (3mm) sensor pad.

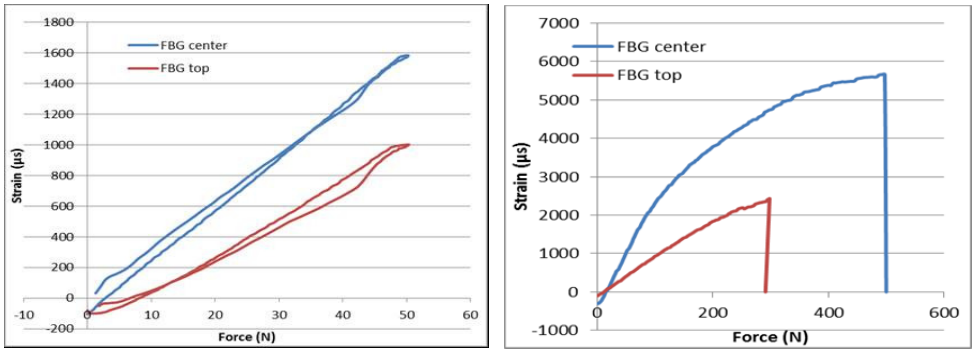

(a) (b)

Figure 8. 2mm specimen a) FBG center/top sensitivity graph for b) FBG center/top dynamic range

4.4.3. Fiber type study

The aforementioned results show that the optimum configuration for thickness/embodiment depth is when FBGs are embedded in the center of a 3mm thick PDMS sheet. Figure 10 presents the results obtained for hydrogenated SMF-28 fiber FBG sensors and non-hydrogenated GF1B fiber FBG respectively for this optimum configuration. We notice a 20% increased sensitivity for the hydrogenated fiber but with a 40% decrease in dynamic range when compared to the non-hydrogenated fiber.

To summarize the case studies, we have identified the basic manufacturing parameters that enhance the sensor pads rigidity and durability to guarantee their reliability in biomedical applications such as medical beds, wheelchairs and amputee sockets. We have performed an analysis of the fabrication parameters and concluded that the optimum sensor pad layout that enhances durability and preserves required sensitivity is fiber embodiment at the polymer center with thickness of 3mm non-hydrogenated fiber.

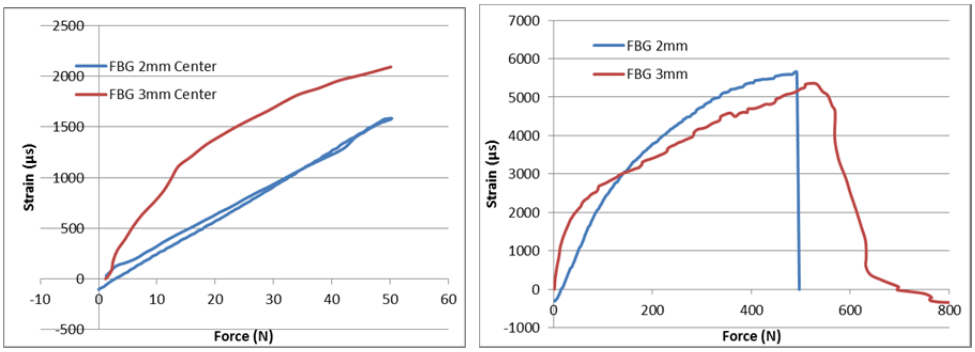

(a) (b)

Figure 9. 2mm specimen a) FBG center/top sensitivity graph for b) FBG center/top dynamic range

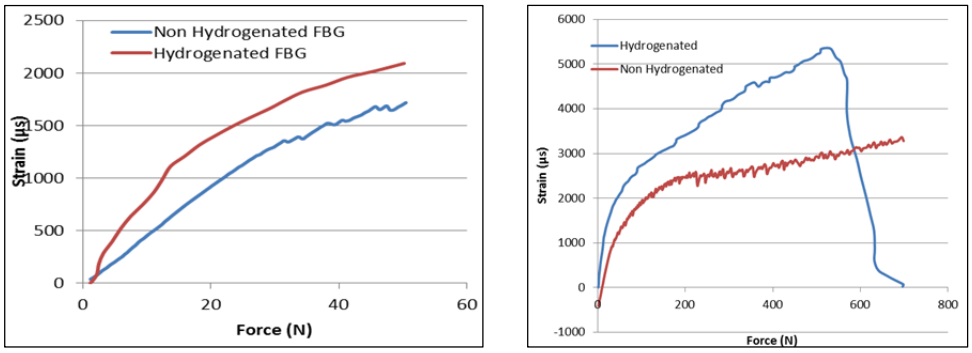

(a) (b)

Figure 10. 3mm specimen a) Hydrogenated/non hydrogenated fiber sensitivity graph for b) dynamic range

5. Application perspective studies

5.1. Pressure monitoring requirements in prosthetics

An assistive device with unresolved sensing challenges is the prosthetic socket. There are well over 32 million amputees in the world, nearly 60% of which being trans-tibial (19.2 million), 75% of which (14.4 million) are complaining of discomfort or significant reduction of autonomy and mobility mainly due to poor socket fit and the resulting development of pressure ulcers (WHO 2010 world report [33]). Project SMARTSocket (SMARTSocket: FP7-PEOPLE- IAPP Grant agreement 251649) deals with the comprehensive understanding and quantification of the differences between two socket interventions (Elevated Vacuum -EV vs Total Surface bearing-TSB-A), leading to some important conclusions:

Given the up to date depth of this investigation (80 patients) several interesting findings were reported: (1) A new socket-stump assessment method revealed for the first time the

magnitude of true shear occurring within the socket in dynamic activities (jumping-running, pivoting); (2) max skin deformation did not correlate with max loading rates during strenuous activities; Maximum stump sliding-slippage reached levels of up to 15 cm (aver. 8± 7cm) while max residual bone pistoning reached values of 19 cm (aver. 12± 7cm) [65]-[71]. Stump skin deformations exceeded 20% of resting length and translated to skin stretching of up to 5± 4cm in average depending on the stump area (distal-proximal). Most interestingly strenuous activities revealed stump localized maximal accelerations exceeding 3Gs (39.8 m/s2 for running) suggesting very high previously unrecorded localized force gradients.

In addition, in a series of recent studies [33], [54]-[64] direct pressure was measured with an appropriately instrumented socket that showed interface pressures to approximately 415 kPa and resultant shear stresses to approximately 65kPa [55], [56]. As a reference, peak pressure on the stump during walking typically range from 700 to 870 kPa pressure [58] and peak shear stresses from 24 to 70kPa. Shear management was out of the scope of this study; however shear values were measured for further kinematics and biomechanics analysis.

5.2. Pressure monitoring requirements in medical beds and seating systems

Project IASiS (FP 7-SME-Grant Agreement 232479) responded to a pan-European Pressure ulcer survey showing prevalence higher than 25% in bedridden and wheelchair bound patients [33], [2] IASiS addressed pressure ulcer incidence and treatment by developing and demonstrating an Intelligent Adaptable Surface envisaged to be capable of redistributing the pressure applied on the skin in bedridden patients or wheelchair users. This adaptable mechanism comprises of self-shaping actuator-driven elements and is responsible for relieving pressure in a timely manner according to the information received by the sensing modules. The IASiS sensors were designed to detect the magnitude of pressure events, and feed it back to the active controllers of the hospital bed/seat surface. The most important result from the clinical trials in IASiS (benchmarked also against the literature) was some more definite operational boundaries for the sensor. The interface pressures on different types of hospital bed mattresses or specialty beds were: 62-107±15mmHg (8.3-14.3kPa) for the areas of Sacrum when semi-recumbent, backrest at 45%; 6-156±22mmHg (8.1-20.8kPa) at the trochander when side lying, hips and knees at 60 degrees; 107-213±17mmHg (14.3-28.4 KPa) on the heels in supine lying; and 60-146±12mmHg (8-19.5 kPa) in the inchial tuberocities when sitting on 10cm standard cushion.

5.3. Sensors per application

Table 4 represents the full sensor specifications tree. Specifically the table summarizes the outcomes of research projects and studies regarding the targeted characteristics of a pressure sensor in order to comply with the requirements of three rehabilitation interventions. It becomes apparent that the most demanding application both in terms of dynamic range as well as flexibility and sampling rate is the prosthetic socket. That is due to its deployment by the patient in every day activities including highly strenuous actions. In the contrary the medical bed is more demanding in sensitivity and that is due to the micro loading dynamics developed in the long run at the skin-mattress interface of a bed-ridden patient.

Functionality, Type of activity to be detected	**Limited motion, low speed-low load, large duration events**	**Moderate relative motion, speed, moderate loading and medium duration events**	**High relative motion, high speed, impact type loading, small duration events**
Clinical Application	**Specialty Hospital Bed Acute Rehab**	**Wheelchair Seats**	**Amputee Sockets (Highly Strenuous Activities)**
Full Scale output Pressure (kPa)	Pressure: 0-40kPa	Pressure: 0-300kPa	Pressure: 0-1MPa
Accuracy	Pressure: <10 Pa	Pressure: <1 kPa	Pressure: <1 KPa
Unit sensor size	$2cm^2$	$1cm^2$	$1cm^2$
Thickness	<4mm	<5mm	<5mm
Flexibility (Bending radius)	4cm	2cm	2cm
Sensitivity	Pressure: 5 Pa	Pressure: 10 Pa	Pressure: 10 Pa
Sampling rate	>15Hz	>50Hz	>400Hz
Hysteresis	Negligible	Negligible	Negligible

Table 4. The sensor specification tree per application and functionality versus characteristics and operational ranges.

6. Conclusion

The embodiment of FBG inscripted optical fibers in polymer 2D surfaces allows for functional and durable pressure sensor configurations meeting specific requirements claimed by specific rehabilitation interventions at the human machine interface. We have developed an optical fiber based 2D pressure sensor exhibiting a high sensitivity of 10% optical power loss per 10kPa pressure and a high spatial resolution of $1cm^2$. The sensing elements have a real-time response and demonstrated no hysteresis as the cyclic measurements demonstrated, while their operation is independent, yielding a 1:1 correlation of each FBG sensor indication to the respective sensing point without the need of data post-processing and allowing for easy pressure pattern identification in multi-point operation. The presented 2x2 cm^2 sensing surface is easily expandable and can be used as a building block for larger scale sensors depending on the application. The mechanical properties of the presented sensor pad allow for embedding or attaching the sensor to irregular shapes and geometries, offering enhanced response to curvature while the low physical dimension commercially available interrogation unit enhances the portability features of the complete sensing system. The sensor's minimal thickness, make it very unobtrusive, with minimal interference on the measurement interface. These attractive physical and operational characteristics are ideally suited for biomedical applications in biomechanics, rehabilitation and orthotics such as amputee sockets and wheelchair/hospital bed -system sensors. In addition, we have identified the basic manufacturing parameters that enhance the sensor pads rigidity and durability to guarantee their reliability in the abovementioned biomedical applications Comparative studies showed that the optimum

sensor pad layout that enhances durability and preserves required sensitivity is fibre embodiment at the polymer centre with thickness of 3mm non-hydrogenated fibre. Finally we have identified and categorized the specifications of the developed sensing surface that will meet the requirements imposed by the specific applications.

Author details

Dimitris Tsiokos and George T. Kanellos
Informatics and Telematics Institute, Center for Research and Technology Hellas, Thessaloniki, Greece

George Papaioannou
S.S.F. Safe Smart Fabric Adaptable Surface Ltd, Nicosia, Cyprus

Stavros Pissadakis
Institute of Electronic Structure and Laser, Foundation for Research and Technology Hellas, Heraklion, Greece

Acknowledgement

The work presented here was partially supported by EU-FP7-SME-2008-1, No 232479,– IASiS and SMARTSocket: FP7-PEOPLE- IAPP Grant agreement 251649.

7. References

[1] American Pressure Ulcer Advisory Panel (1998). Pressure ulcer Prevalence, cost and risk assessment: consensus development conference statement. Decubitus 2:24-8
[2] Pezzin, L.E., Dillingham, T.R., Mackenzie, E.J., Ephraim, P. and Rossbach, P., (2004). "Use and satisfaction with prosthetic limb devices and related services". Arch Phys Med Rehabil, May, 85(5),pp. 723-9.
[3] Petrovic, S.J., Dobb, H., Mezentsev, K.V., Kalli, K.M., IEEE, , Webb, J.D.M., IEEE, and Bennion, I.M., (2007). "Sensitivity of LPGs in PCFs Fabricated by an Electric Arc to Temperature, Strain, and External Refractive Index". Journal of lightwave technology, 25(5).
[4] Murphy, P.R., James, W.S. and Tatam, P.R., (2007). "Multiplexing of Fiber-Optic Long-Period Grating-Based Interferometric Sensors". Journal of lightwave technology, March, 25(3).
[5] Mignani, G.A. and Baldini, F., (1997). "Fibre-optic sensors in health care". Phys. Med. Biol. , 42,pp. 967-979.
[6] Mignani, G.A. and Baldini, F., (1996). "Biomedical sensors using optical fibres". Rep. Prog. Phys, 59,pp. 1-28.
[7] Huang, C.Y., Wang, W.C., Wu, W.J. and Ledoux, R.W., (2007). "Composite Optical Bend Loss Sensor for Pressure and Shear Measurement". IEEE SENSORS JOURNAL, 7(11).
[8] Kim, S.H. and Lee, J.J., (2003). "Phase-Shifted Transmission/Reflection-Type Hybrid Extrinsic Fabry–Pérot Interferometric Optical Fiber Sensors". Journal of lightwave technology, March, 21(3),pp. 797.

[9] Geernaert, T., Luyckx, G., Voet, E., Nasilowski, T., Chah, K., Becker, M., Bartelt, H., Urbanczyk, W., Wojcik, J., De Waele, W., Degrieck, J., Terryn, H., Berghmans, F. and Thienpont, H., (2009). "Transversal Load Sensing With Fiber Bragg Gratings in Microstructured Optical Fibers". IEEE Photonics Technology Letters, 1 January, 21,pp. 6-8.

[10] Kanellos, T.G., Mitrogiannis, C., Nianios, G., Pleros, N. and Papaioannou , G., (2009). "High spatial resolution FBG-array based strain sensor". Proceedings of the International Commission for Optics (ICO) Topical Meeting on "Emerging Trends and Novel Materials in Photonics", Delphi, Greece, October 7-9.

[11] Gusarov, A., Chojetzki, C., Mckenzie, I., Thienpont, H. and Berghmans, F., (2008). "Effect of the fiber coating on the radiation sensitivity of type IFBGs". IEEE Photonics Technol. Lett, 20,pp. 1802-1804.

[12] Pressure sensors: selection and applications by DUANE TANDESKE. (Edt).MARCEL DEKKER Inc., New York(1990) ISBN 0-8247-83-65-4.

[13] Sensors in Biomedical Applications Fundamentals technology and applications: Gabor HarsaNyi CRC press (2000) ISBN 1-566760885-3.

[14] Handbook of Modern Sensors 3rd Edition. Jacob Fraden (Edt): Springer (2003) ISBN-10: 0-387-00750-4

[15] Sensors and actuators in mechatronics Andrzej M. Pawlak. CRC- Taylor and Francis(2007) ISBN-10: 0-8493-9013-3

[16] Cork, R. (2007): XSENSOR technology: a pressure imaging overview. Sensor Review, vol. 27 pp. 24-28.

[17] Van Drongelen, S., Van der Woude, L. H., Janssen, T. W., Angenot, E. L., Chadwick, E. K. and Veeger, D. H. (2005): Mechanical load on the upper extremity during wheelchair activities. Arch Phys Med Rehabil, vol. 86(6), Jun, pp. 1214-1220.

[18] Appoldt, F.A., Bennett, L. and Contini, R., (1969). "Socket pressure as a function of pressure transducer protrusion". Bulletin of Prosthetics Research, Spring,pp. 236-249.

[19] Sanders, J.E. and Daly, C.H., (1993). "Measurement of stresses in the three orthogonal directions at the residual limb-prosthetic socket interface". IEEE Trans Rehabil Eng 1(2),pp. 79-85.

[20] Convery, P. and Buis, A.W., (1998). "Conventional patellar-tendon-bearing (PTB) socket/stump interface dynamic pressure distributions recorded during the prosthetic stance phase of gait of a trans-tibial amputee". Prosthet Orthot Int, Dec, 22(3),pp. 193-8.

[21] Convery, P. and Buis, A.W., (1999). "Socket/stump interface dynamic pressure distribution recorded during the prosthetic stance phase of gait of a trans-tibial amputee wearing a hydrocast socket". Prosthet Orthot Int, Aug, 23(2),pp. 107-112.

[22] Engsberg, J.R., Springer, M.J.N. and Harder, J.A., (1992). "Quantifying interface pressure in below-knee-amputee socket". Journal Association of Children's Prosthetic-Orthotic Clinics 27(3),pp. 81-88.

[23] Houston, V.L., Mason, C.P., LaBlanc, K.P., Beatties, A.C., Garbarini, M.A. and Lorenze, E.J., (1994). "Preliminary results with the DVA-Tekscan BK prosthetic socket/residual limb stress measurement system". Proceedings of the Proceedings of 20th Annual Meeting American Academy of Orthotist and Prosthetist, Nashville, TN,pp. 8-9.

[24] Sanders, J.E., Daly, C.H. and Burgess, E.M., (1993). "Clinical measurement of normal and shear stresses on a trans-tibial stump: characteristics of wave-form shapes during walking". Prosthet Orthot Int, Apr, 17(1),pp. 38-48.

[25] Zhang, M., Turner-Smith, A.R., Tanner, A. and Roberts, V.C., (1996). "Frictional action at residual limb/prosthetic socket interface". Med Eng Phys, 18(3),pp. 207-214.
[26] Polliack, A.A., Landsberger, S., McNeil, D.R., Sieh, R.C., Craig, D.D. and Ayyappa, E., (1999). "Socket measurement systems perform under pressure". Jounal of Biomechanics, June,pp. 71-80.
[27] Polliack, A.A., Sieh, R.C., Craig, D.D., Landsberger, S., McNeil, D.R. and Ayyappa, E., (2000). "Scientific validation of two commercial pressure sensor systems for prosthetic socket fit". Prosthet Orthot Int, Apr, 24(1),pp. 63-73.
[28] Brimacombe, J.M., Anglin, C., Hodgson, A.J. and Wilson, D.R., (2005). "Validation of Calibration Techniques for TEKSCAN Pressure Sensors." Proceedings of the XXth ISB Congress - 29th ASB Annual Meeting, Cleveland, Ohio, July 31st-August 5th.
[29] Cork, R., (2007). "XSENSOR technology: a pressure imaging overview". Sensor Review, 27(1),pp. 24-28.
[30] Hadcock, L., Stevenson, J., Morin, E., Bryant, T., Reed, S., Abdoli, M. and Tasker, T., (2007). "Pressure Measurement Applications for Humans". Queen's University, Fergenbaum Mitchell School of Rehabilitation Queen's University, Kingston, Ontario.
[31] Papaioannou, G., Protopappas, V.C., Glaros, C., Morres, I. and Tsopelas, P., (2005). "Tekscan pressure sensor equilibration and conditioning". Proceedings of the 3rd European Medical & Biological Engineering Conference, Prague, Czech republic, November 20-25, 2005.
[32] Pramanik, C., Saha, H. and Gangopadhyay, U., (2006). "Design optimization of a high performance silicon MEMS piezoresistive pressure sensor for biomedical applications,". Journal of Micromechanics and Microengineering, 16,pp. 2060-2066.
[33] Bader D. Et., al. (2010) Pressure ulcer Research. Current and Future Perspectives. (eds) Springer Verlag Berlin ISBN-13 978-3-642-06404-3.
[34] 22Papaioannou, G., Protopappas, C.V., Tsopelas, P., Mitrogiannis, C., Nianios, G. and Tashman, S., (2008), "A new Method for pressure sensor Equilibration and conditioning" Br. Journal of Biomotricity, 2(3), pp. 176-195.
[35] J. W. Arkwright, N. G. Blenman, I. D. Underhill, and S. A. Maunder, M. M. Szczesniak, P. G. Dinning, and I. J. Cook, "In-vivo demonstration of a high resolution optical fiber manometry catheter for diagnosis of gastrointestinal motility disorders", Opt. Express, Vol. 17, No. 6, 16 March 2009, pp. 4500-4506
[36] Chu-Yu Huang, Wei-Chih Wang, Member, IEEE, Wen-Jong Wu, and William R. Ledoux "Composite Optical Bend Loss Sensor for Pressure and Shear Measurement", IEEE Sensors Journal, VOL. 7, NO. 11, pp. 1554-1565, 2007
[37] Francis Berghmans, "Photonic skins for optical sensing: highlights of the PHOSPHOS project", in Optical Fiber Sensor Congference - OFS-20, Technical Digest (CD) (Optical Society of America, 2009), paper OF101 08.
[38] H. M. Xie, Ph. Dabkiewicz, R. Ulrich, and K. Okamoto. Side-hole fiber for fiber-optic pressure sensing. Opt. Lett., 11:333–335, 1986.
[39] C. Jewart, K. P. Chen, B. McMillen, M. M. Bails, S. P. Levitan, J. Canning, and I. V. Avdeev. Sensitivity enhancement of fiber bragg gratings to transverse stress by using microstructural fibers. Optics letters, 31(15):2260–2262, 2006.

[40] T. Martynkien, M. Szpulak, and W. Urbanczyk. Modeling and measurement of temperature sensitivity in birefringent photonic crystal holey fibers. Appl. Opt., 44:7780–7788, 2005.

[41] W. J. Bock and W. Urbanczyk. Measurements of sensitivity of birefringent holey fiber to temperature, elongation, and hydrostatic pressure. In Proc. of the 21st IEEE-Instrumentation and Measurement Technology Conference, volume 2, pages 1228–1232, Como, Italy, 2004.

[42] D. Kim and J. U. Kang. Sagnac loop interferometer based on polarization maintaining photonic crystal fiber with reduced temperature sensitivity. Opt. Express, 12:4490–4495, 2004.

[43] CH. L. Zhao, X. Yang, Ch. Lu, W. Jin, and M.S. Demokan. Temperatureinsensitive interferometer using a highly birefringent photonic crystal fiber loop mirror. IEEE Photon. Tech. Lett., 16:2535–2537, 2004.

[44] T. Martynkien, G. Statkiewicz, M. Szpulak, J. Olszewski, G. Golojuch,W. Urbanczyk, J.Wojcik, P. Mergo, M. Makara, T. Nasilowski, F. Berghmans, and H. Thienpont. Measurements of polarimetric sensitivity to temperature in birefringent holey fibers. Meas. Sci. Technol., 18:3055–3060, 2007.

[45] G. T. Kanellos, G. Papaioannou, D. Tsiokos, C. Mitrogiannis, G. Nianios, and N. Pleros, "Two dimensional polymer-embedded quasi-distributed FBG pressure sensor for biomedical applications," Opt. Express 18, pp. 179-186, 2010.

[46] C. Yan, E. Ferraris, T. Geernaert, F. Berghmans, D. Reynaerts, Development of flexible pressure sensing polymer foils based on embedded fibre Bragg grating sensors, Procedia Engineering, Volume 5, Eurosensor XXIV Conference, Eurosensor XXIV Conference, pp. 272-275, 2010.

[47] http://www.ibsen.dk/products/im/I-MON-80D-Interrogation-monitor

[48] G. T. Kanellos, G. Papaioannou, D. Tsiokos, C. Mitrogiannis, G. Nianios, and N. Pleros, "Two dimensional polymer-embedded quasi-distributed FBG pressure sensor for biomedical applications," Opt Express 18, 179-186 (2010).

[49] C. Jewart, K. Chen, B. McMillen, M. Bails, S. Levitan, J. Canning and I. Avdeev, “Sensitivity enhancement of fiber Bragg gratings to transverse stress by using microstructural fibers,” Optics Letters, V. 31, No. 15, pp. 2260-2262 (2006).

[50] S. Pissadakis and M. Konstantaki, "Photosensitivity of germanosilicate fibers using 213nm, picosecond Nd : YAG radiation," Opt Express 13, 2605-2610 (2005).

[51] Kanellos, G.T.; Tsiokos, D.; Pleros, N.; G. Papaioannou, Childs, P.; Pissadakis, S.; “Enhanced durability FBG-based sensor pads for biomedical applications as human-machine interface surfaces”, BioPhotonics, 2011 International Workshop on, 8-10 June 2011, page(s): 1 – 3, Parma, Italy.

[52] Albert, B. Malo, K. O. Hill, F. Bilodeau, D. C. Johnson, and S. Theriault, "Comparison of One-Photon and 2-Photon Effects in the Photosensitivity of Germanium-Doped Silica Optical Fibers Exposed to Intense Arf Excimer-Laser Pulses," Appl Phys Lett 67, 3529-3531 (1995).

[53] J. Albert, K. O. Hill, D. C. Johnson, F. Bilodeau, S. J. Mihailov, N. F. Borrelli, and J. Amin, "Bragg gratings in defect-free germanium-doped optical fibers," Opt Lett 24, 1266-1268 (1999).

[54] Sonk WA, et.al., (1970) Effect of liner materials on interface pressure in below knee prosthesis. Arch Phys Med Rehabil 51:666-669.

[55] Pollick AA, et.al., (2002) Laboratory and clinical tests of a proptotype pressure sensor for clinical ssessment of prosthetic socket fit (prost Ortht Int 26:23-34.
[56] Sanders JE., (1995) Interface mechanics in external prosthetics: review of interface stress measurement techniques. Med Biol. Eng Vomput 33:509-516.
[57] Lowe LB., et.al., Suction-socket pressure in lower extremity prosthesis. J Niomech. 1:247-257.
[58] Armstrong DG. Et. al. (1998) Is there a critical level of plantar foot pressure to identify patients at risk for neuropathic foot ulceration? J Foot Ankle Surg 37:303-307.
[59] Hosein R., et.al., (2000) A study of in-shoe plantar shear in normals. Clin. Biomech 15:46-53.
[60] Appoldt FA., et.al., (1998) stump-socket pressure in lower extremity prosthesis. J biomech 1:247-257.
[61] Sanders JE. et. al., (1998)Effects of alignment changes on stance phase pressures and shear stresses on trans-tibial amputees: measurements from 13 transducer sites IEEE trans Rehab Eng 6:21-31.
[62] Naylor PDF (1955) Experimental friction blisters BR J Dermat 67:327-342.
[63] Pearson JR., et.al., (1973) Pressures in critical regions of the below knee patellar tendon bearing prosthesis. Bull Prosth Res 10-19:52-76.
[64] Burgess EM, et.al., (1977) /a study of interface pressures in the below knee prosthesis (physiological suspension: and interim report). Bull Prosthe res 10-28:58-70.
[65] Papaioannou, G.,Tsiokos D., Fiedler G., Kanelos G.T., Mitrogiannis, C., Avdeev I., Wood J. and McKinney R. (2010). "Dynamic radiography imaging as a tool in the design and validation of a novel intelligent amputee socket", J.M.R.S. Tavares and R.M.N. Jorge (eds.), Computational Vision and Medical Image Processing: Recent Trends, Computational Methods in Applied Sciences 19, DOI 10.1007/978-94-007-0011-6 5,_c Springer Science+Business Media B.V. 2011.
[66] Papaioannou, G., Mitrogiannis, C., Nianios, G. and Fiedler, G., (2010). "Assessment of amputee socket-stump-residual bone kinematics of strenuous activities using Dynamic Roentgen Stereogrammetric Analysis". Journal of Biomechanics; 43(2010) 871-878.
[67] Papaioannou, G., Nianios, G., Mitrogiannis, C. and Fiedler, G., (2010). "Assessment of internal and external prosthesis kinematics during strenuous activities using Dynamic Roentgen Stereophotogrammetric Analysis". Journal of Prosthetics and Orthotics, 22:1-15.
[68] Papaioannou, G., Fiedler, G., Mitrogiannis, and C. Nianios, G., (2010). "In-vivo velocity and acceleration characteristics of trans-tibial amputee socket-stump interaction during strenuous activities", Journal of Rehabilitation Research, ACCEPTED March 2010.
[69] Papaioannou, G., Fiedler, G., Mitrogiannis, C., Nianios, G., (2010). "Amputee skin deformation maps using Dynamic Roentgen Stereogrammetric imaging". Computational Vision and Medical Image Processing, ISBN: 978-0-415-57041-1. CRC Press: pp. 236-247.
[70] George Papaioannou, Christos Mitrogiannis, George Nianios and Goeran Fiedler. "Assessment of Vacuum-assisted trans-tibial amputee socket dynamics" (2010), International Journal for Computational Vision and Biomechanics, 8(3), pp.271-284.
[71] Papaioannou, G., Mitrogiannis, C., Nianios, G. and Fiedler, G., (2009). "Tracking high speed arthrokinematics using a new and high resolution Biplane Dynamic Roentgen Stereogrammetric method". International Journal of Imaging, 2:(A09) pp. 66-85.